Molecular Vision 2017; 23:872-888 <http://www.molvis.org/molvis/v23/872>
Received 13 August 2017 | Accepted 3 December 2017 | Published 5 December 2017

The retina/RPE proteome in chick myopia and hyperopia models: Commonalities with inherited and age-related ocular pathologies

Nina Riddell,[1] Pierre Faou,[2] Melanie Murphy,[1] Loretta Giummarra,[1] Rachael A. Downs,[2] Harinda Rajapaksha,[2] Sheila G. Crewther[1]

[1]Department of Psychology and Counselling, School of Psychology and Public Health, La Trobe University, Melbourne, VIC, Australia; [2]Department of Biochemistry and Genetics, La Trobe Institute for Molecular Sciences, La Trobe University, Melbourne, VIC, Australia

Purpose: Microarray and RNA sequencing studies in the chick model of early optically induced refractive error have implicated thousands of genes, many of which have also been linked to ocular pathologies in humans, including age-related macular degeneration (AMD), choroidal neovascularization, glaucoma, and cataract. These findings highlight the potential relevance of the chick model to understanding both refractive error development and the progression to secondary pathological complications. The present study aimed to determine whether proteomic responses to early optical defocus in the chick share similarities with these transcriptome-level changes, particularly in terms of dysregulation of pathology-related molecular processes.

Methods: Chicks were assigned to a lens condition (monocular +10 D [diopters] to induce hyperopia, −10 D to induce myopia, or no lens) on post-hatch day 5. Biometric measures were collected following a further 6 h and 48 h of rearing. The retina/RPE was then removed and prepared for liquid chromatography-electrospray ionization-tandem mass spectrometry (LC-ESI-MS/MS) on an LTQ-Orbitrap Elite. Raw data were processed using MaxQuant, and differentially abundant proteins were identified using moderated *t* tests (fold change ≥1.5, Benjamini-Hochberg adjusted $p<0.05$). These differentially abundant proteins were compared with the genes and proteins implicated in previous exploratory transcriptome and proteomic studies of refractive error, as well as the genes and proteins linked to the ocular pathologies listed above for which myopia or hyperopia are risk factors. Finally, gene set enrichment analysis (GSEA) was used to assess whether gene sets from the Human Phenotype Ontology database were enriched in the lens groups relative to the no lens groups, and at the top or bottom of the protein data ranked by Spearman's correlation with refraction at 6 and 48 h.

Results: Refractive errors of −2.63 D ± 0.31 D (mean ± standard error, SE) and 3.90 D ± 0.37 D were evident in the negative and positive lens groups, respectively, at 6 h. By 48 h, refractive compensation to both lens types was almost complete (negative lens −9.70 D ± 0.41 D, positive lens 7.70 D ± 0.44 D). More than 140 differentially abundant proteins were identified in each lens group relative to the no lens controls at both time points. No proteins were differentially abundant between the negative and positive lens groups at 6 h, and 13 were differentially abundant at 48 h. As there was substantial overlap in the proteins implicated across the six comparisons, a total of 390 differentially abundant proteins were identified. Sixty-five of these 390 proteins had previously been implicated in transcriptome studies of refractive error animal models, and 42 had previously been associated with AMD, choroidal neovascularization, glaucoma, and/or cataract in humans. The overlap of differentially abundant proteins with AMD-associated genes and proteins was statistically significant for all conditions (Benjamini-Hochberg adjusted $p<0.05$), with over-representation analysis implicating ontologies related to oxidative stress, cholesterol homeostasis, and melanin biosynthesis. GSEA identified significant enrichment of genes associated with abnormal electroretinogram, photophobia, and nyctalopia phenotypes in the proteins negatively correlated with ocular refraction across the lens groups at 6 h. The implicated proteins were primarily linked to photoreceptor dystrophies and mitochondrial disorders in humans.

Conclusions: Optical defocus in the chicks induces rapid changes in the abundance of many proteins in the retina/RPE that have previously been linked to inherited and age-related ocular pathologies in humans. Similar changes have been identified in a meta-analysis of chick refractive error transcriptome studies, highlighting the chick as a model for the study of optically induced stress with possible relevance to understanding the development of a range of pathological states in humans.

Myopia currently affects 23% of the world's population, and its prevalence is rising. Approximately 4.8 billion people (50% of the population) are predicted to be myopic by 2050, nearly 1 billion of whom will be highly myopic [1]. This poses a significant public health and socioeconomic challenge, as myopia (and high myopia in particular) increases risk for a range of sight-threatening pathologies, including cataract, glaucoma, and chorioretinal abnormalities [2-4]. Hyperopia also alters the risk of pathological complications,

Correspondence to: Sheila G. Crewther, School of Psychology and Public Health, La Trobe University, Plenty Road, Bundoora, VIC, Australia, 3083; Phone: +61 3 9479 2290; FAX: +61 3 9479 1956; email: S.Crewther@latrobe.edu.au

with several studies associating shorter axial length and/or hyperopic refraction with angle closure glaucoma and age-related macular degeneration (AMD) [3-6].

The mechanisms linking refractive errors with ocular complications are poorly understood; however, it is broadly thought that the gross structural features of myopia and hyperopia play a causative role. For example, the shorter axial length of hyperopic eyes may cause abnormalities in the size and position of anterior structures that increase risk for angle closure glaucoma [4,7,8]. Comparatively, the mechanical stress associated with distension of the vitreous chamber in myopia causes thinning and tractional changes within posterior ocular layers that potentially predispose the eye to chorioretinal abnormalities, such as retinal breaks, lacquer cracks, and posterior staphyloma [9-11]. Ultrastructural studies have demonstrated that profound myopia induction over several weeks in the chick model is sufficient to produce pathological chorioretinal abnormalities similar to those observed following decades of high myopia in humans [12-15]. During the first 4 weeks of occlusion myopia induction in the chick, cone outer segment membranes show increasingly severe signs of disruption and degeneration [16], and RPE cells become thinner and lose their basal infoldings [16-18]. The RPE nuclei and mitochondria also become irregular in shape [16,18], and the dispersion of the mitochondria and melanin granules within the cell becomes dysregulated [16]. Retinal folds and detachment have been reported when occlusion is prolonged longer than 4 weeks [19], and by 8 weeks, lacquer crack lesions are observed in the majority of occluded chicks [20]. In humans, these lesions predispose the development of choroidal neovascularization, which affects 5–11% of those with high myopia [2,13].

The biologic processes linked with the onset and progression of refractive error also involve genes known to be associated with the development of pathological states. The genes implicated in genome-wide association studies of refractive error in humans have pleiotropic effects in non-ocular systems where the genes are linked to a range of disorders, including diabetes, and neuropsychiatric and developmental conditions [21]. Our recent transcriptome meta-analysis [22] also demonstrated significant overlap between the genes differentially expressed within the first three days of optically induced refractive error in the chick model and the genes and proteins associated with several pathologies for which myopia or hyperopia are risk factors (AMD, choroidal neovascularization, and cataract). Curiously, the overlap did not show strong specificity for the sign of ocular growth, suggesting that the non-specific features of optically induced refractive error in chicks (such as blur, loss of form vision, peripheral occlusion, or heat under the goggle) may be a sufficient source of physiological stress to induce rapid expression changes in pathology-associated genes.

Although changes in gene expression during the first 3 days of refractive error induction in the chick model have been extensively researched using discovery-driven microarray, RNA sequencing, and meta-analysis techniques, relatively little is known about the corresponding proteome changes [23]. Thus, in the present study, we aimed to determine whether early proteomic responses to optical defocus in the chick correspond well with early transcriptome changes, particularly in terms of dysregulation of pathology-associated genes. Protein abundance changes in the retina/RPE were profiled using liquid chromatography-electrospray ionization-tandem mass spectrometry (LC-ESI-MS/MS) following 6 and 48 h of optically induced myopia and hyperopia in the chick. Differentially abundant proteins were compared with the genes and proteins implicated in previous refractive error studies, as well as those associated with ocular pathologies for which myopia and hyperopia are known risk factors. To assess pathology-related genes from a more exploratory perspective, we also used gene set enrichment analysis (GSEA) to determine whether any Human Phenotype Ontology gene sets were enriched in the lens groups relative to the no lens groups, or at the top or bottom of the protein list ranked by correlation with ocular refraction.

METHODS

Animals and rearing: Thirty-one male chicks (Leghorn/New Hampshire), obtained from a commercial hatchery, were raised from post hatch days 0–4 under a 12 h:12 h light-dark cycle. On post-hatch day 5, chicks were randomly assigned to a lens condition (+10 or −10 diopters [D], or no lens), and lenses (polymethyl methacrylate) attached to Velcro were fixed to the periocular feathers of the right eye. Separate no lens control animals were used because monocular treatments in chicks can affect blood flow [24,25], refraction, and axial length [26] in the contralateral eye. Lensing was staggered so that the two tissue collection time points were circadian matched; the chicks in group 1 were lensed 3 h into the light cycle, and the chicks in group 2 were lensed 9 h into the light cycle. All procedures adhered to the ARVO Statement for the use of Animals in Ophthalmic and Vision Research and were conducted in accordance with approved La Trobe University Animal Ethics Committee protocols.

Ocular biometry and tissue collection: Following 6 h (group 1) or 48 h (group 2) with the lenses attached, the chicks were anesthetized (ketamine, 45 mg/kg; xylazine, 4.5 mg/kg i.m.), and the right eye refraction and axial dimensions

were determined with retinoscopy (Keeler, Vista Diagnostic Instruments, Windsor, UK) and A-Scan ultrasonography (7 MHz probe; A-Scan III, TSL: Teknar, Inc., St Louis, MO). Biometric measures were collected for five chicks per condition, with the exception of the 6 h negative lens condition where biometry could not be performed on one animal due to anesthesia effects and the 48 h no lens condition where six chicks were profiled. The chicks were then euthanized via decapitation, and their right eyes were enucleated. The section of retina/RPE between the ora serrata and 1 mm temporal to the pecten was removed under a surgical microscope (OPMI 1-FC; Zeiss, Jena, Germany), frozen in liquid nitrogen, and transferred to a −80 °C freezer. The time from initial anesthesia to tissue freezing ranged from 5 to 10 min, the order of tissue collection was counterbalanced across lens groups, and all tissue was collected in a single batch within 1 h of the designated time point (6 or 48 h).

Protein extraction, digestion, and LC-ESI-MS/MS: Retina/RPE samples were resuspended in digestion buffer (8 M urea, 50 mM ammonium bicarbonate, and 10 mM DTT) and incubated for 5 h at 25 °C. Samples were then centrifuged for 15 min at 14,000 ×*g*, and the soluble fraction was used to determine the protein concentrations (Pierce 660 nm Protein Assay, Rockford, IL). Each sample (50 µg protein) was adjusted to 100 µl with digestion buffer, and 55 mM iodoacetamide was then added to the alkylate thiol groups at 20 °C for 35 min in the dark. The alkylated preparation was diluted to 1 M urea with 25 mM ammonium bicarbonate (pH 8.5) before sequencing-grade trypsin (Promega, Madison, WI) was added to the 5 µM final concentration. Digests were performed overnight at 37 °C. The digests were acidified with 1% (v/v) trifluoroacetic acid (TFA) and the peptides desalted on SDB-XC Empore StageTips (3M Company, St. Paul, MN), as previously described [27]. Peptides were reconstituted in 0.1% TFA and 2% acetonitrile (ACN), and 1 µg was loaded onto C_{18} PepMap 100 µm ID × 2 cm trapping columns (Thermo Fisher Scientific, San Jose, CA) at 5 µl/min for 6 min, and washed for 6 min before the precolumn was switched in line with the analytical column (Vydac MS C_{18}, 3 µm, 300 Å and 75 µm ID × 25 cm, Grace Pty. Ltd., Columbia, MD). The peptides were separated at 300 nl/min using a nonlinear ACN gradient of buffer A (0.1% formic acid and 2% ACN) and buffer B (0.1% formic acid and 80% ACN), starting at 5% buffer B to 55% over 120 min. Data were collected on an Orbitrap Elite (Thermo Fisher Scientific) in Data Dependent Acquisition mode using m/z 300–1,500 as the MS scan range. Collision induced dissociation (CID) MS/MS spectra were collected for the 20 most intense ions per MS scan. Dynamic exclusion parameters were set as follows: repeat count 1, duration 90 s, and the exclusion list size was set at 500 with early expiration disabled. Other instrument parameters for the Orbitrap were MS scan at 120,000 resolution, maximum injection time 50 ms, AGC target 1×10^6, and CID at 35% energy for a maximum injection time of 150 ms with an AGT target of 5,000. The Orbitrap Elite was operated in dual analyzer mode with the Orbitrap analyzer used for MS and the linear trap used for MS/MS.

Biometric data analysis: One-way ANOVA tests using SPSS for Windows (Version 20, IBM Corp, Armonk, NY) were conducted to compare the effects of lens-wear (negative, positive, and no lens) on the refraction, axial length, and vitreous chamber depth at each time point. Tukey honest significant difference (HSD) post-hoc tests were used as required, and p values of less than 0.05 were considered statistically significant. All dependent variables were normally distributed (Shapiro-Wilks test $p>0.05$ and/or skewness and kurtosis within the acceptable range) and met the assumption of equal variances (Levene's test $p>0.05$).

LC-ESI-MS/MS data preprocessing: Identification and quantification of proteins were performed on raw output files from LC-ESI-MS/MS using MaxQuant (Version 1.5.1.6 [28,29]) and the built-in Andromeda search engine with the *Gallus gallus* UniProt FASTA database (September 2016) and common contaminants. Carbamidomethylation of cysteines was set as a fixed modification, and acetylation of protein N-termini and methionine oxidation were included as variable modifications. Parent mass tolerance was set to 5 ppm after refinement by MaxQuant, and fragment mass tolerance to 0.5 Da. Trypsin was set as the digestion enzyme with up to two missed cleavages allowed. Peptides with a minimum of seven amino-acid length were considered, and the false discovery rate (FDR) was set to 1% at the peptide and protein levels. The match-between-runs feature was used to transfer peptide identifications from one run to another based on the retention time and the mass to charge ratio. The Max LFQ algorithm [29] was used for label-free protein quantification.

Normalized protein group ratios obtained from MaxQuant were log2 transformed. Flagged protein groups (i.e., potential contaminants, reverse proteins, and those identified only by site) and protein groups with more than 40% missing values in any experimental condition were filtered from the results. The remaining missing values (comprising 2.51% of the data) were imputed using the hybrid QRLIC/SVD approach implemented in the imputeLCMD R package (v2.0). The data set was then normalized using the Cyclic Loess function in the Linear Models for Microarray Data R package (LIMMA; v3.30.12 [30]). Protein ANalysis THrough Evolutionary Relationships (PANTHER, v12) [31] gene ontology and protein class classifications for the 1,617

proteins remaining in the data set following filtering, imputation, and normalization are provided in Appendix 1.

Identification of differentially abundant proteins: Empirical Bayes moderated *t* tests (LIMMA R package v3.30.12) were used to identify differentially abundant proteins in the lens groups relative to no lens groups at each time point and the negative lens groups relative to positive lens groups at each time point. Protein groups displaying a fold change of greater than or equal to 1.5 (log2 FC ≥0.585) and Benjamini-Hochberg [32] adjusted p value of less than 0.05 were considered differentially abundant.

Identification of human orthologs: To enable comparisons with previous studies in other species and the use of curated human gene set files for GSEA, high confidence human orthologs for each Uniprot Accession in the data set were identified using InParanoid (v8.0) [33]. InParanoid employs a reciprocal best hits approach that performs well in benchmarking tests of orthology inference [34]. As orthologs could not be matched for all proteins, the data set used for the subsequent GSEA contained 1,327 identifiers. As a final step, human ortholog Uniprot IDs for the differentially abundant proteins were matched to human Ensembl gene IDs using Biomart (*Homo sapiens* GRCh38.p7) [35].

Comparison with previous transcriptome and proteomic studies: Differentially abundant proteins were compared with previous exploratory proteomic and transcriptome studies of optically induced refractive error as follows. Lists of genes and proteins implicated in transcriptome and proteomic studies published before July 2016 were obtained from Riddell and Crewther's supplemental materials [23]. As part of this previous study, the gene and protein lists were mapped to human ortholog Ensembl Gene IDs to enable cross-species and cross-platform comparisons. We performed a PubMed search on June 17, 2017, to update the lists with studies published after July 2016. Of the three studies published since this time [36-38], only two provided lists of implicated genes that could be used in the present analysis [37,38]. The genes implicated in these two studies were mapped to human ortholog Ensembl Gene IDs using the methods reported in our previous publication [23]. We then compared the updated gene and protein lists with differentially abundant proteins from the present study mapped to human Ensembl gene IDs. Chord diagrams were created to display the overlapping gene and protein findings using the GOplot R package (v1.0.2) [39]. Appendix 2 summarizes the methods used in each of the previous studies included in the comparison.

Comparison with the genes and proteins associated with ocular pathologies in humans: We also compared the differentially abundant proteins from the present study with genes and proteins previously associated with ocular pathologies in humans. Author-curated lists of genes associated with primary open angle glaucoma (POAG), choroidal neovascularization, cataract, sub-clinical AMD, and AMD in humans (either via genetic linkage or association or RNA or protein expression changes) were sourced from recent publications and converted to Ensembl Gene IDs using BioMart (Ensembl release 86; *Homo sapiens* GRCh38.p7) as described previously [22]. The pathology-associated lists were then compared with differentially abundant proteins from the present study using the R software package GeneOverlap (v1.10.0). This package uses Fisher's exact test to calculate the significance of overlap between each pair of lists in comparison to the genomic background. The function returns the number of intersecting findings between the two lists, the p value, and the estimated odds ratio. The null hypothesis is that the odds ratio is no larger than 1; values larger than this odds ratio indicate a positive association between lists. A contingency table was created to display the pairwise overlaps between protein and pathology lists, including the number of intersecting genes, odds ratios, and significant Benjamini-Hochberg adjusted p values. A chord diagram was created to display the overlapping gene and protein findings using the *GOplot* R package (v1.0.2) [39].

STRING database analyses: Lists of differentially abundant proteins of particular interest were further explored using the STRING database (v10.5) functional enrichment tool [40]. This analysis identified gene ontologies and pathways that were overrepresented in the protein lists relative to the *Homo sapiens* genomic background.

Gene set enrichment analyses: GSEA was used to assess Human Phenotype Ontology [41,42] gene set enrichment in the lens groups relative to the no lens groups and in the protein data ranked by correlation with refraction. For the first analysis, a *Homo sapiens* Human Phenotype Ontology UniProt gene set file was obtained from the Bader laboratory on June 17, 2017 [43], and imported into the javaGSEA app [44] along with the data set of normalized log transformed label-free quantification (LFQ) intensity values mapped to human ortholog UniProt IDs. GSEA was then used to assess Human Phenotype Ontology gene set expression in the lens groups relative to the no lens groups at each time point. The signal-to-noise metric was used to rank proteins by the difference of the class means scaled by the standard deviation, and gene set enrichment at the top and bottom of the ranked lists was determined using 1,000 gene set permutations and an FDR q value cut-off of 0.05.

For the second analysis, correlations between refraction and normalized LFQ protein intensities across the negative lens, no lens, and positive lens groups at each time point

were calculated using Spearman's rho (Hmisc R package). The 6 h and 48 h protein lists ranked by correlation with refraction were then imported into the javaGSEA app [44], and GSEA was conducted using the preranked metric and 1,000 gene set permutations as described above. Leading-edge subset analysis was then used to identify the subset of proteins responsible for gene set enrichment (i.e., proteins that appeared in the ranked list at or before the point at which the running sum reached its maximum deviation from zero).

RESULTS

Refraction and axial dimension changes: The ocular biometry measurements are illustrated in Figure 1A–C. Refractive shifts were evident in both lens groups at 6 h, and by 48 h compensation to the negative and positive 10 D lenses was almost complete (Figure 1A). One-way ANOVAs indicated that refraction was statistically significantly different between the lens groups at 6 h ($F(2,11) = 68.215$, $p<0.001$) and at 48 h ($F(2,13) = 637.470$, $p<0.001$). Post-hoc tests revealed that the refractive state of all lens groups was significantly different at both time points ($p<0.01$ for all comparisons). There were no statistically significant differences in the axial dimensions between the lens groups at 6 h (Figure 1B). By 48 h, however, the lens groups differed statistically significantly in axial length ($F(2,13) = 8.413$, $p = 0.005$) and vitreous chamber depth ($F(2,13) = 8.539$, $p = 0.004$). Post-hoc tests revealed that the axial length was statistically significantly shorter in the positive lens group relative to the negative lens group ($p = 0.003$) and that the vitreous chamber depth was statistically significantly shorter in the positive lens group relative to the no lens ($p = 0.039$) and negative lens ($p = 0.004$) groups. As expected, there was a strong negative correlation between the refraction and ocular axial dimensions (Figure 1C).

Protein abundance changes: The negative and positive lens groups were first compared with age-matched no lens controls to identify differentially abundant proteins at each time point. At 6 h, 144 proteins were differentially abundant in the negative lens group, and 163 proteins were differentially abundant in the positive lens group. At 48 h, 149 proteins were differentially abundant in the negative lens group, and 173 were differentially abundant in the positive lens group. Of these differentially abundant proteins, 72 were either up- or downregulated in both lens groups at 6 h (Figure 2A), and 67 were either up- or downregulated in both lens groups at 48 h (Figure 2B). To identify abundance changes that were sensitive to the sign of defocus, we next compared the negative and positive lens groups directly at each time point. No proteins were differentially abundant between the negative and positive lens groups at 6 h, and only 13 were differentially abundant at 48 h (Figure 2C). Appendix 3 provides a detailed overview of the proteins implicated in each comparison.

Overlap with previous proteomic and transcriptome studies of refractive error: Comparison of these differentially abundant proteins with the findings of previous exploratory transcriptome and proteomic studies of refractive error revealed several commonalities. Eleven of the 390 proteins identified as differentially abundant in the present study have been implicated in previous proteomic studies (Figure 3A). This relatively low number of commonalities may reflect the use of gel electrophoresis in most previous studies, as well as differences in the species, tissues, and time points profiled (see Appendix 2). In contrast, 55 of the 390 differentially abundant proteins have been implicated in previous transcriptome studies where the methodological conditions often matched those of the present study more closely (Figure 3B,C). We also compared our findings with the results of a previous transcriptome meta-analysis, which analyzed the subset of refractive error transcriptome studies conducted in the chick model. This comparison identified another ten unique commonalities with the present proteomic findings (and 12 commonalties in total; Figure 3B). Thus, 65 of the 390 differentially abundant proteins from the present study have previously been implicated at the transcriptome level (53 in individual transcriptome studies, ten in the chick transcriptome meta-analysis, and two in individual studies and the meta-analysis).

We tested each set of commonalities for over-representation of gene ontologies and pathways relative to the *Homo sapiens* background. No ontologies or pathways were significantly over-represented in the commonalities with previous proteomic studies. A large number of ontologies related to structural processes were over-represented in the transcriptome commonalities (Appendix 4), with the most significant over-representation occurring for the 'axonogenesis' ontology. Additionally, several ontologies related to melanin were over-represented in the transcriptome meta-analysis commonalities (Appendix 5). We also conducted an over-representation analysis for the remaining list of differentially abundant proteins that were not implicated in any previous transcriptome studies. Three hundred and ninety-eight ontologies and pathways were over-represented (Appendix 6). The most significant gene ontologies were related to extracellular vesicles, and the most significant pathways were ribosome and spliceosome.

Overlap with pathology-associated genes and proteins: Our previous meta-analysis of chick transcriptome data sets demonstrated overlap between differentially expressed genes in the chick model of early (i.e., ≤3 days) optically induced

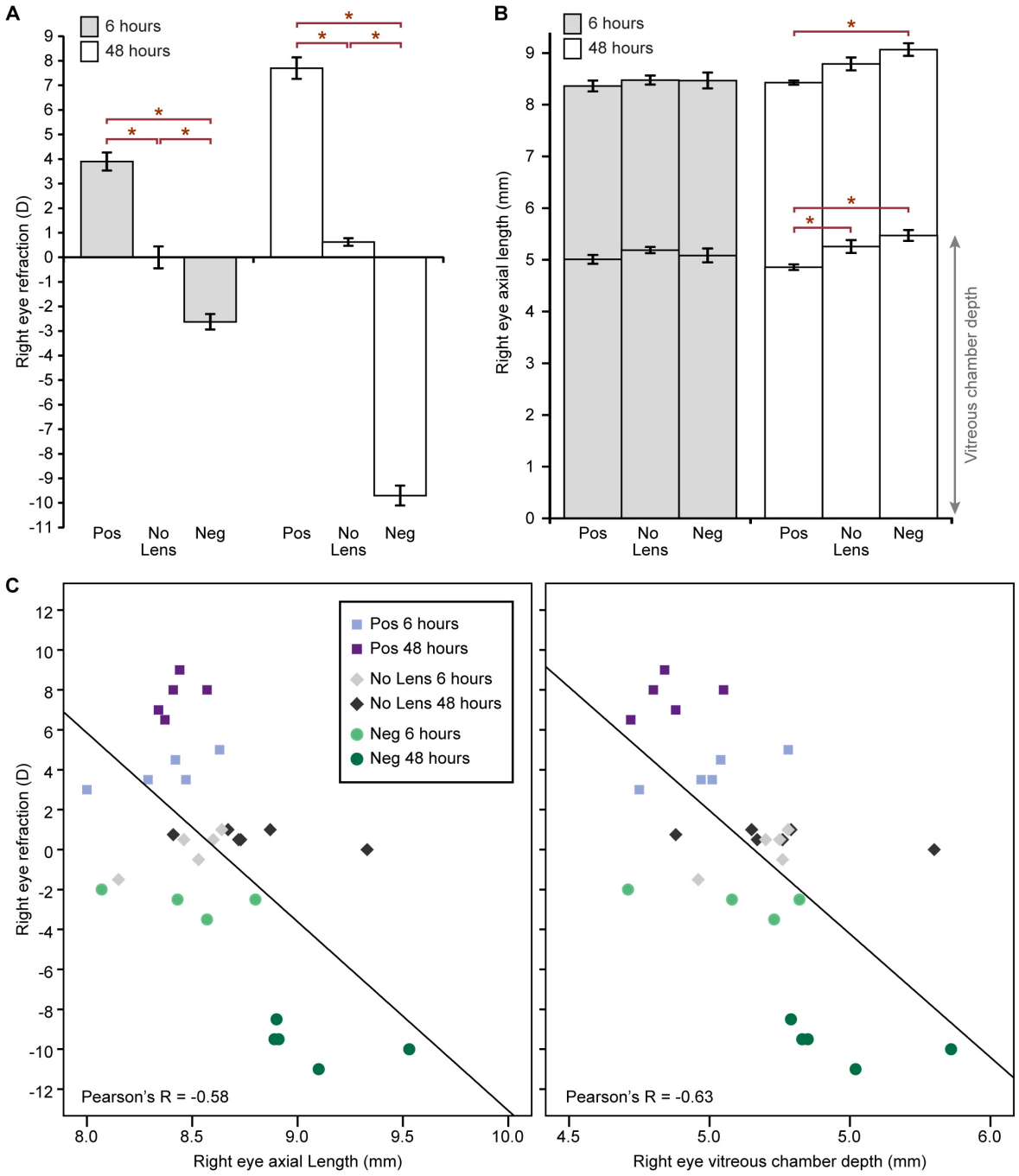

Figure 1. Ocular biometry measurements. Column charts show the mean (± standard error, SE) right eye (**A**) refraction and (**B**) axial length following 6 and 48 h of lens-wear or no lens rearing. Mean vitreous chamber depth (± SE) is indicated at the bottom of each axial length column. **C**: Scatter plots show the relationship between the refraction and ocular axial dimensions (the axial length and the vitreous chamber depth). Neg = negative lens, Pos = positive lens.

refractive errors and the genes and proteins previously linked to a range of ocular pathologies for which myopia or hyperopia are risk factors (POAG, choroidal neovascularization, cataract, sub-clinical AMD, and AMD [22];). To test whether a similar association occurs at the protein level, we compared the same pathology-associated gene and protein lists with the differentially abundant proteins from the present study.

As illustrated in Figure 4A, the genes and proteins linked to AMD in humans overlapped statistically significantly with differentially abundant proteins following 6 and

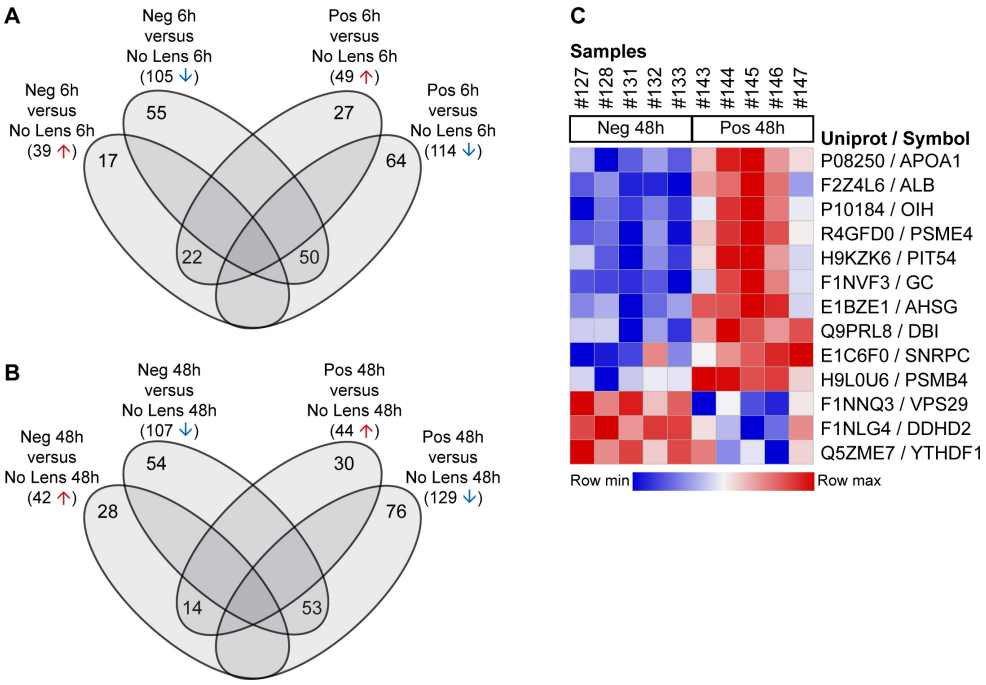

Figure 2. Protein abundance changes across lens groups at 6 and 48 h. Venn diagrams show the overlap of differentially abundant proteins in positive and negative lens groups relative to age-matched no lens controls at (**A**) 6 h and (**B**) 48 h. **C**: Heat map showing the label-free quantification (LFQ) intensity of individual samples for the 13 proteins that were differentially abundant between the negative and positive lens groups at 48 h. Neg = negative lens, Pos = positive lens.

48 h of negative and positive lens-wear in the chick model. The overlap with AMD-associated genes and proteins was greatest at late relative to early time points, and in the negative relative to the positive lens-group (negative 6 h odds ratio [OR] = 8.36, p<0.001; negative 48 h OR = 10.19, p<0.001; positive 6 h OR = 4.49, p = 0.002; positive 48 h OR = 4.79, p = 0.001). The differentially abundant proteins following 48 h of negative lens-wear also overlapped statistically significantly with the genes and proteins linked to choroidal neovascularization (OR = 14.20, p = 0.008). A range of ontologies were over-represented in the protein-pathology overlaps as a whole (Appendix 7). The most significant over-representation was blood microparticles (FDR<0.001). Ontologies related to physiologic stress, cholesterol homeostasis, and melanin were also implicated (Figure 4B).

Correlation of human disease phenotype gene sets with refraction: In addition to comparing the overlap of differentially abundant proteins with specific ocular-pathology associated gene/protein lists, we used GSEA to assess whether any gene sets from the Human Phenotype Ontology database were enriched in response to lens-wear. This analysis tested whether the genes from any Human Phonotype Ontology gene sets were over-represented near the top or bottom of the ranked protein lists. Two methods were used to rank the proteins. In the first approach, categorical comparisons between the lens and no lens conditions at each time point were made by ranking proteins by the difference of class means scaled by the standard deviation. No significant enrichments were identified using this approach. In the second approach, proteins were ranked by Spearman's correlation with refraction across groups at 6 h and 48 h. No significant enrichments were found in the 48 h analysis; however, at 6 h, abnormal electroretinogram, photophobia, and nyctalopia gene sets were enriched in the proteins negatively correlated with refraction, and the arrhythmia gene set was enriched in the proteins positively correlated with refraction (Table 1).

The leading-edge subsets of the abnormal electroretinogram, nyctalopia, and photophobia gene sets were highly similar and were primarily comprised of genes associated with retinal dystrophies and mitochondrial diseases (Figure 5). Consistent with these disease associations, a range of photoreceptor-related proteins were implicated, including those involved in phototransduction (OPN1LW, GUCA1A, and CNGB1), vitamin A metabolism (RPE65 and RLBP1), photoreceptor disc morphogenesis (FSCN2), protein trafficking within photoreceptors (UNC119), and photoreceptor-controlled retinal organization (RS1). The remaining leading-edge proteins were primarily related to mitochondrial function (TIMM8A, SLC25A4, and MT-CO2) and pre-mRNA splicing (PRPF4 and PRPF8). The final disease phenotype showing a significant correlation with refraction was arrhythmia. Two of the four leading-edge proteins from this phenotype gene set (GNAQ and GNA11) are associated with melanocyte development and melanopsin signaling. Mutations in these genes and NRAS (the third leading-edge protein) have been linked to melanoma in humans. The final

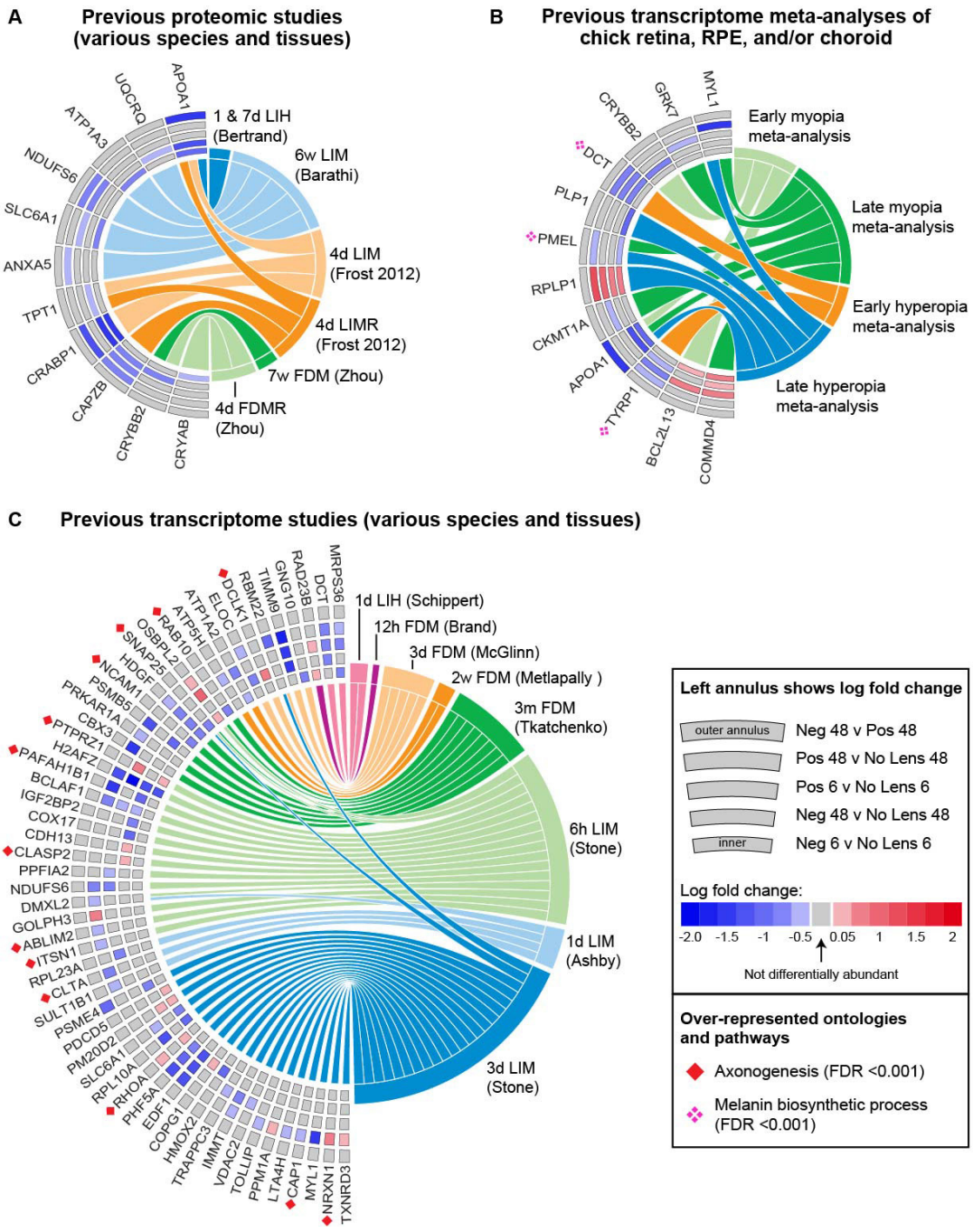

Figure 3. Comparison of differentially abundant proteins with previous exploratory proteomic and transcriptome studies of refractive error. **A**: Chord diagram showing the 11 proteins that were differentially abundant in the present study and differentially abundant in previous proteomic studies. **B**: Chord diagram showing the 12 proteins that were differentially abundant in the present study and differentially expressed in previous meta-analyses of chick refractive error transcriptome studies. **C**: Chord diagram showing the 55 proteins that were differentially abundant in the present study and differentially expressed in previous transcriptome studies. The fold change of individual proteins in the present study is shown on the left side of each chord diagram, with the position in the annulus indicating the condition. Previous studies implicating the same protein and gene are shown on the right. Protein contributions to the most significant ontology over-representations (melanin biosynthetic process and axonogenesis) are indicated with symbols. Appendix 2 and Appendix 8 provide further details on all previous studies included in these comparisons. Neg = negative lens, Pos = positive lens, h = hours, d = days, w = weeks, m = months, LIH = lens-induced hyperopia, LIM = lens-induced myopia, FDM = form deprivation myopia, LIMR = LIM recovery, FDMR = FDM recovery.

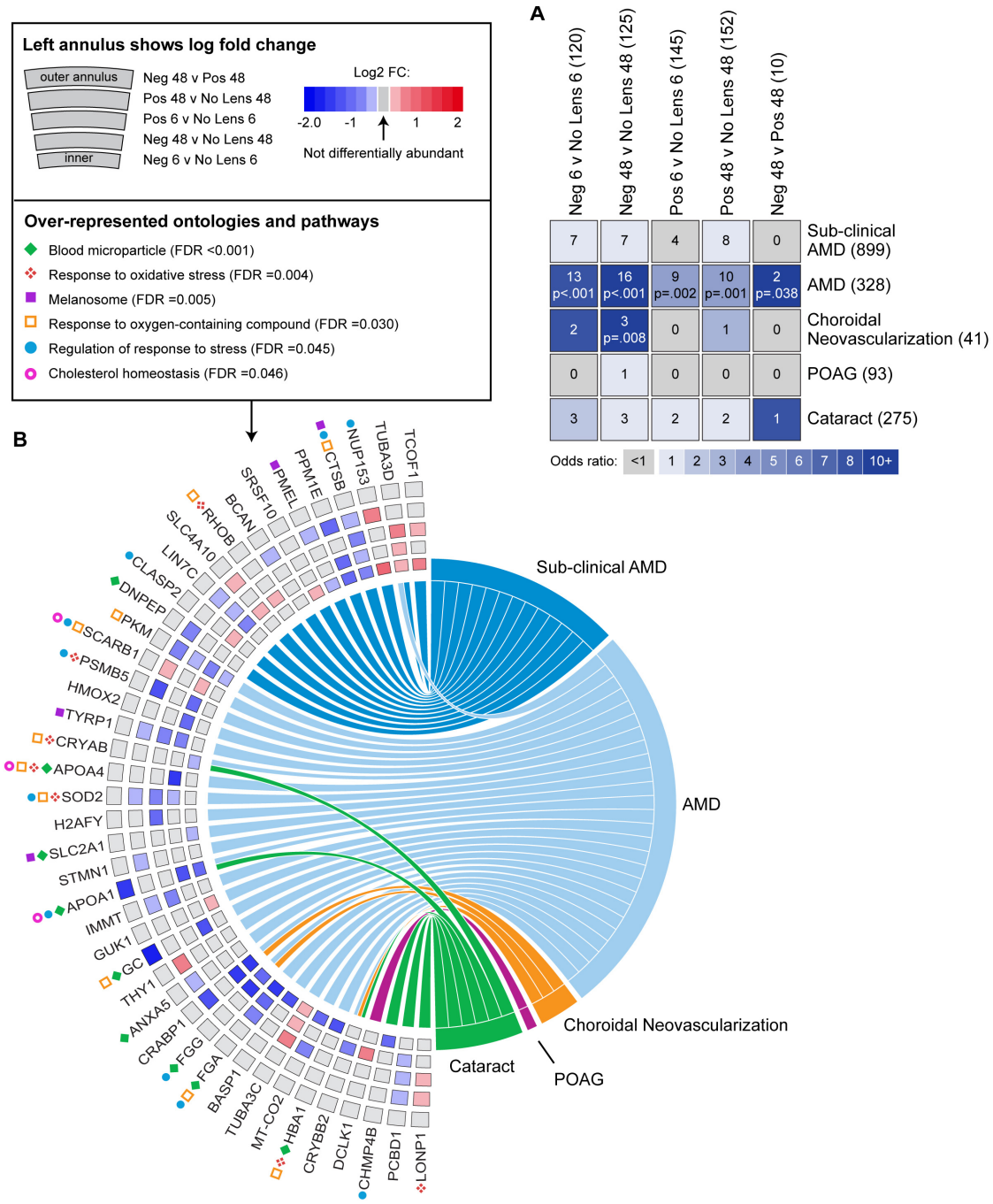

Figure 4. Comparison of single protein findings with the genes and proteins linked to ocular pathologies in humans. **A**: Table showing overlap between differentially abundant proteins in the present study and the genes and proteins previously associated with sub-clinical AMD, AMD, choroidal neovascularization, POAG, and cataract in humans. The number of genes and proteins in each list is shown in parentheses after the list name. List intersections (i.e., the number of overlapping findings) and Benjamini-Hochberg adjusted p values are superimposed on the grid. **B**: Chord diagram showing the individual genes and proteins that were differentially abundant in the present study and associated with an ocular pathology (i.e., all intersecting genes and proteins from Figure 4A). The fold change of individual proteins in the present study is shown on the left side of the chord diagram, with the position in the annulus indicating the condition. Left-right connections indicate protein associations with ocular pathologies. Protein contributions to a subset of significant ontology over-representations are indicated with symbols in panel **B**. Neg = negative lens, Pos = positive lens, AMD = age-related macular degeneration, POAG = primary open angle glaucoma.

protein, A2ML1, is a protease inhibitor involved in innate immunity.

DISCUSSION

This study is the first to use a high throughput proteomic approach to characterize early responses to optical defocus in an animal model of refractive error. The results demonstrate that proteomic responses to lens-wear are well under way by 6 h in the chick model, with more than 140 differentially abundant proteins identified in both lens groups. Moreover, the response to negative and positive lenses was highly similar at both time points (with only 13 proteins showing sign-of-defocus dependent abundance changes at 48 h). Overall, the implicated proteins showed improved concordance with the findings of previous transcriptome studies in animal models of refractive error, and substantial commonalities with the genes and proteins linked to inherited and age-related ocular pathologies in humans.

A key aim of this study was to identify commonalties between transcriptome and proteome responses to optically induced refractive error. The majority of transcriptome studies to date have profiled retina, RPE, and/or choroid tissue in the first 3 days of refractive error induction in the rapid chick model [37,45-48]. Conversely, most previous proteomic studies profiled protein abundance in the retina or sclera at later induction time points in slower animal models, such as the guinea pig [49,50], tree shrew [51,52], and mouse [53,54]. Given the diverse methodologies used, it is not surprising that our previous systematic comparison identified only 20 commonalities between the findings of all transcriptome and proteomic studies in the field [23]. By comparison, 65 of the 390 differentially abundant proteins from the present study have previously been identified as differentially expressed at the transcriptome level [22,38,45-48,55,56]. This substantial improvement likely reflects the use of a high throughput proteomic method and the better alignment of our methodological conditions with the transcriptome data in terms of the species, time points, and tissues profiled.

Although the concordance of our proteomic results with earlier transcriptome findings is undoubtedly improved, it is still relatively low given that some of the transcriptome data were generated using similar animal models to the present study (see Appendix 2 and Appendix 8). Translation and protein degradation rates also contribute to protein abundance, and these processes have been shown to primarily affect proteins performing basic cellular and housekeeping functions following stimulation [57]. This is consistent with the over-representation of ribosome and spliceosome proteins in our list of differentially abundant proteins that were not implicated in any previous transcriptome studies. It is also likely that a range of factors decreased the number of transcriptome-proteome commonalities in the present data comparison. Changes in the abundance of proteins with a long half-life can correlate best with mRNA abundance changes several hours earlier [57]. Thus, it is possible that some of the protein abundance changes in the 6 h data reflect mRNA changes in the relatively unstudied [55] hours immediately following application of the lens. The conversion of all data to a common identifier in the present study necessarily resulted in some loss of information (e.g., when orthologs could not be identified), and systematic biases in high-throughput platforms are also known to obscure a substantial proportion of the correlation between the mRNA and protein levels [58]. The contribution of mRNA levels to protein abundance has been shown to be high once these measurement biases are accounted for, particularly during responses to a stimulus [57,59].

The transcriptome-proteome commonalities that we identified were enriched for structural (particularly neuronal cell growth) and melanin biosynthesis ontologies, indicating that transcriptional regulation of these processes is to some extent reflected at the protein abundance level. Differential expression of genes and proteins involved in regulating cellular structure is an expected and common finding given the morphological features of refractive errors [22,37,56,60-64]. The evidence for melanin biosynthesis dysregulation in refractive error models is more limited. Mutations in the master transcription factor for melanogenesis, MIFT, are associated with microphthalmia in a range of animals [65,66]. MIFT controls the transcription of the three melanin biosynthesis genes that were differentially expressed in our previous meta-analysis of chick transcriptome studies [22]

Table 1. Human Phenotype Ontologies enriched in the proteins correlated with refraction at 6 h.

Ontology	Ontology identifier	Normalized enrichment score	FDR
Photophobia	HP:0000613	−1.93	0.042
Nyctalopia	HP:0000662	−1.97	0.034
Abnormal electroretinogram	HP:0000512	−2.00	0.050
Arrhythmia	HP:0011675	2.03	0.030

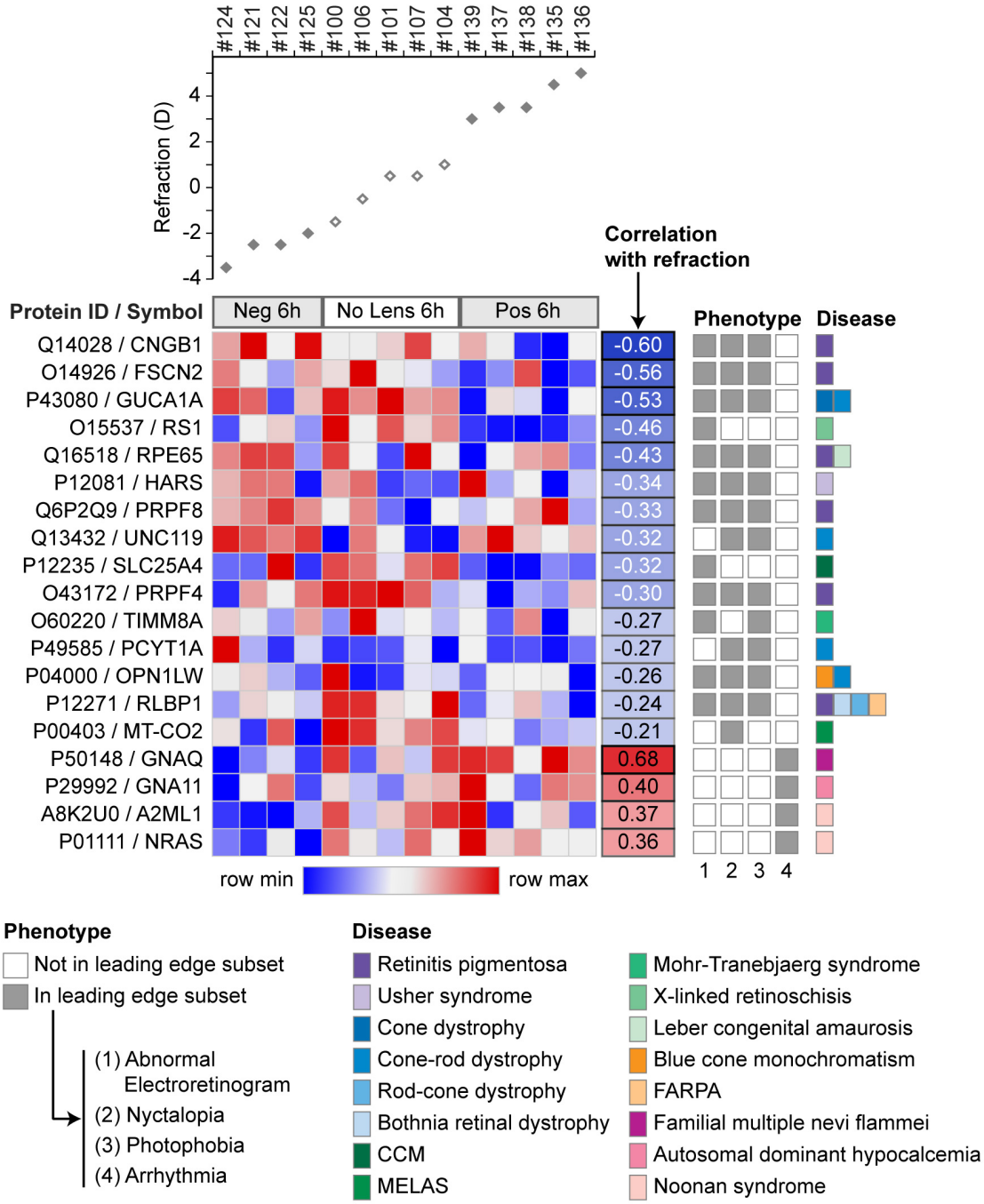

Figure 5. Leading-edge subset proteins from the Human Phenotype Ontology gene sets implicated at 6 h. The heat map shows the leading-edge proteins from the four gene sets that were significantly enriched at the top or bottom of the protein list ranked by correlation with refraction at 6 h (abnormal electroretinogram, nyctalopia, photophobia, and arrhythmia). Heat map intensity values are plotted below the corresponding refraction measure for each sample. The panels to the right show the correlation of individual proteins with refraction, and provide further information on phenotype and disease associations (as listed in the Human Phenotype Ontology database; human-phenotype-ontology.github.io/). CCM = congenital cataract-hypertrophic cardiomyopathy-mitochondrial myopathy syndrome, MELAS = mitochondrial myopathy, encephalopathy, lactic acidosis, and stroke-like episodes, FARPA = fundus albipunctatus retinitis punctata albescens.

and downregulated at the protein level during myopia and hyperopia induction in the present study (DCT, PMEL and TYRP1 [67];). More broadly, albinism is known to impair emmetropization in humans [68,69] and is associated with myopia in guinea pigs [70] and chicks [71]. The melanogenesis pathway also interacts with a range of signaling processes that have previously been associated with ocular growth regulation and refractive errors, including retinoic acid, Wnt, nitric oxide, dopamine, bFGF, and TGF-beta [67,72,73].

In addition to implicating melanin biosynthesis genes, our meta-analysis of chick transcriptome studies identified differential expression of a range of complement pathway and oxidative stress genes during refractive error induction [22]. There was no evidence for complement pathway activation at the protein level in the present study, perhaps because of the earlier time point profiled (2 days versus 2–3 days) or the tissue composition (retina/RPE versus the retina/RPE/choroid). However, a range of proteins that regulate or respond to oxidative stress were either upregulated (RHOB [74], LONP1 [75], CPEB2 [76], and SLC8A1 [77]) or downregulated (PSMB5 [78,79], CRYAB [80], APOA4 [81], SOD2 [82,83], HBA1 [84,85], PRNP [86], AKR1B1 [87], MAPT [88], NQO1 [89], RPS3 [90], and GPR37L1 [91]) following defocus. Melanin and oxidative stress pathways have been linked to AMD and choroidal neovascularization pathogenesis in humans [92-94], and a substantial proportion of the genes and proteins implicated in our meta-analysis [22] and the present study have been directly associated with these pathologies. The pattern of overlap with pathology-associated genes was similar at the transcriptome and proteome level; greater commonality with AMD and choroidal neovascularization genes was evident at later time points and during myopia (relative to hyperopia) induction, and many of the commonalities were not specific for the sign of defocus (i.e., the genes and proteins were up or downregulated during myopia and hyperopia induction).

A further untargeted analysis of all Human Phenotype Ontology gene sets identified enrichment of genes linked to abnormal electroretinogram, nyctalopia, and photophobia phenotypes in the proteins negatively correlated with refraction at 6 h. The implicated genes were primarily associated with photoreceptor dystrophies and mitochondrial disorders in humans. Early shifts in phototransduction and mitochondrial metabolism pathways have also been reported at the mRNA level in chicks, though not always in a sign-of-defocus-dependent manner [37]. Inherited retinal dystrophies in humans are associated with an increased incidence of refractive errors, particularly if they affect the photoreceptors or the bipolar synapse [95]. A recent conference abstract also reported that such genes that produce refractive error as part of a broader syndrome are enriched for polymorphisms associated with common myopia in the CREAM and 23andMe genome-wide association data [96], suggesting that the molecular mechanisms implicated in these disorders are relevant for understanding the basis of refractive errors in the general population.

Although changes within mitochondrial, phototransduction, melanin, and oxidative stress pathways have been linked to ocular pathologies in humans, it is unclear whether this is the case in the chick optical defocus model as little is known about the longitudinal ultrastructural and molecular effects of lens-wear [23,62]. The relevance of the identified protein abundance changes to human refractive error and associated secondary complications is also uncertain. As noted in our earlier investigation [22], the disruption of gene and protein expression within oxidative stress pathways could reflect the secondary effects of lens-wear such as peripheral occlusion or increased heat under the goggle. Further ultrastructural and molecular studies to address these questions are warranted, given the many advantages of chick for ophthalmic research [97] and the apparent potential of the model to replicate several of the molecular features of common age-related ocular disorders in humans.

In conclusion, this study compared differentially abundant proteins following 6 and 48 h of lens-wear in the chick with differentially expressed genes and proteins from previously published transcriptome and proteomic studies of refractive error, as well as the genes and proteins associated with several sight-threatening ocular pathologies in humans. The results demonstrate that cellular remodeling, melanin biosynthesis, and oxidative stress pathways are implicated at the mRNA and protein levels in animal models of refractive error. The improved concordance of the present proteomic findings with previous transcriptome studies highlights the importance of methodological choices for studies aiming to build on the existing literature and contribute to a systems-level understanding of refractive error development. We also demonstrated significant overlap between the differentially abundant proteins following lens-wear and the genes and proteins linked to AMD and choroidal neovascularization in humans. These findings highlight the chick as a model for the study of optically induced stress, with possible relevance to understanding the development of sight-threatening human ocular pathologies.

APPENDIX 1. PANTHER GENE ONTOLOGY (CELLULAR COMPONENT, MOLECULAR FUNCTION, AND BIOLOGICAL PROCESS) AND PROTEIN CLASS CLASSIFICATIONS FOR THE 1617 PROTEINS IN THE FILTERED LC-ESI-MS/MS CHICK RETINA/RPE DATASET.

To access the data, click or select the words "Appendix 1"

APPENDIX 2. PAST TRANSCRIPTOME AND PROTEOMIC STUDIES OF REFRACTIVE ERROR ANIMAL MODELS.

To access the data, click or select the words "Appendix 2"

APPENDIX 3. DIFFERENTIALLY ABUNDANT PROTEINS.

To access the data, click or select the words "Appendix 3"

APPENDIX 4. FUNCTIONAL ENRICHMENTS FOR DIFFERENTIALLY ABUNDANT PROTEINS ALSO IMPLICATED IN PAST TRANSCRIPTOME STUDIES OF OPTICALLY-INDUCED REFRACTIVE ERROR.

To access the data, click or select the words "Appendix 4"

APPENDIX 5. FUNCTIONAL ENRICHMENTS FOR DIFFERENTIALLY ABUNDANT PROTEINS ALSO IMPLICATED IN PREVIOUS TRANSCRIPTOME META-ANALYSES OF OPTICALLY-INDUCED REFRACTIVE ERROR.

To access the data, click or select the words "Appendix 5"

APPENDIX 6. FUNCTIONAL ENRICHMENTS FOR DIFFERENTIALLY ABUNDANT PROTEINS THAT WERE NOT IMPLICATED IN ANY PREVIOUS REFRACTIVE ERROR TRANSCRIPTOME STUDIES.

To access the data, click or select the words "Appendix 6"

APPENDIX 7. FUNCTIONAL ENRICHMENTS FOR DIFFERENTIALLY ABUNDANT PROTEINS ALSO ASSOCIATED WITH HUMAN OCULAR PATHOLOGIES.

To access the data, click or select the words "Appendix 7"

APPENDIX 8. COMPARISON OF SINGLE PROTEIN FINDINGS WITH PAST EXPLORATORY PROTEOMIC AND TRANSCRIPTOME STUDIES OF REFRACTIVE ERROR.

To access the data, click or select the words "Appendix 8"

ACKNOWLEDGMENTS

Funding: This study was supported by an Australian Government Research Training Program Scholarship to NR. SGC (S.Crewther@latrobe.edu.au) and NR (N.Riddell@latrobe.edu.au) are co-corresponding authors for this paper.

REFERENCES

1. Holden BA, Fricke TR, Wilson DA, Jong M, Naidoo KS, Sankaridurg P, Wong TY, Naduvilath TJ, Resnikoff S. Global prevalence of myopia and high myopia and temporal trends from 2000 through 2050. Ophthalmology 2016; 123:1036-42. [PMID: 26875007].
2. Saw SM, Gazzard G, Shih-Yen EC, Chua WH. Myopia and associated pathological complications. Ophthalmic Physiol Opt 2005; 25:381-91. [PMID: 16101943].
3. Flitcroft DI. The complex interactions of retinal, optical and environmental factors in myopia aetiology. Prog Retin Eye Res 2012; 31:622-60. [PMID: 22772022].
4. Shen L, Melles RB, Metlapally R, Barcellos L, Schaefer C, Risch N, Herrinton LJ, Wildsoet C, Jorgenson E. The association of refractive error with glaucoma in a multiethnic population. Ophthalmology 2016; 123:92-101. [PMID: 26260281].
5. Lavanya R, Kawasaki R, Tay WT, Cheung GC, Mitchell P, Saw SM, Aung T, Wong TY. Hyperopic refractive error and shorter axial length are associated with age-related macular degeneration: The singapore malay eye study. Invest Ophthalmol Vis Sci 2010; 51:6247-52. [PMID: 20671287].
6. . Age-Related Eye Disease Study Research Group. Risk factors associated with age-related macular degeneration. A case-control study in the age-related eye disease study: Age-related eye disease study report number 3. Ophthalmology 2000; 107:2224-32. [PMID: 11097601].
7. Wright C, Tawfik MA, Waisbourd M, Katz LJ. Primary angle-closure glaucoma: An update. Acta Ophthalmol 2016; 94:217-25. [PMID: 26119516].
8. Xu L, Cao WF, Wang YX, Chen CX, Jonas JB. Anterior chamber depth and chamber angle and their associations with ocular and general parameters: The Beijing eye study. Am J Ophthalmol 2008; 145:929-36. [PMID: 18336789].
9. Neelam K, Cheung CM, Ohno-Matsui K, Lai TY, Wong TY. Choroidal neovascularization in pathological myopia. Prog Retin Eye Res 2012; 31:495-525. [PMID: 22569156].
10. Curtin BJ. Physiologic vs pathologic myopia: Genetics vs environment. Ophthalmology 1979; 86:681-91. [PMID: 397448].
11. Seko Y, Seko Y, Fujikura H, Pang J, Tokoro T, Shimokawa H. Induction of vascular endothelial growth factor after application of mechanical stress to retinal pigment epithelium of the rat in vitro. Invest Ophthalmol Vis Sci 1999; 40:3287-91. [PMID: 10586955].
12. Avila MP, Weiter JJ, Jalkh AE, Trempe CL, Pruett RC, Schepens CL. Natural history of choroidal neovascularization

in degenerative myopia. Ophthalmology 1984; 91:1573-81. [PMID: 6084222].

13. Ohno-Matsui K, Yoshida T, Futagami S, Yasuzumi K, Shimada N, Kojima A, Tokoro T, Mochizuki M. Patchy atrophy and lacquer cracks predispose to the development of choroidal neovascularisation in pathological myopia. Br J Ophthalmol 2003; 87:570-3. [PMID: 12714395].

14. Vongphanit J, Mitchell P, Wang JJ. Prevalence and progression of myopic retinopathy in an older population. Ophthalmology 2002; 109:704-11. [PMID: 11927427].

15. Hayashi K, Ohno-Matsui K, Shimada N, Moriyama M, Kojima A, Hayashi W, Yasuzumi K, Nagaoka N, Saka N, Yoshida T, Tokoro T, Mochizuki M. Long-term pattern of progression of myopic maculopathy: A natural history study. Ophthalmology 2010; 117:1595-611. [PMID: 20207005].

16. Liang H, Crewther D, Gillard Crewther S, Barila A. A role for photoreceptor outer segments in the induction of deprivation myopia. Vision Res 1995; 35:1217-25. [PMID: 7610583].

17. Hirata A, Negi A. Morphological changes of choriocapillaris in experimentally induced chick myopia. Graefes Arch Clin Exp Ophthalmol 1998; 236:132-7. [PMID: 9498124].

18. Liang H, Crewther SG, Crewther DP, Junghans BM. Structural and elemental evidence for edema in the retina, retinal pigment epithelium, and choroid during recovery from experimentally induced myopia. Invest Ophthalmol Vis Sci 2004; 45:2463-74. [PMID: 15277465].

19. Hayes B, Fitzke F, Hodos W, Holden A. A morphological analysis of experimental myopia in young chickens. Invest Ophthalmol Vis Sci 1986; 27:981-91. [PMID: 3486857].

20. Hirata A, Negi A. Lacquer crack lesions in experimental chick myopia. Graefes Arch Clin Exp Ophthalmol 1998; 236:138-45. [PMID: 9498125].

21. Hysi PG, Wojciechowski R, Rahi JS, Hammond CJ. Genome-wide association studies of refractive error and myopia, lessons learned, and implications for the future. Invest Ophthalmol Vis Sci 2014; 55:3344-51. [PMID: 24876304].

22. Riddell N, Crewther SG. Novel evidence for complement system activation in chick myopia and hyperopia models: A meta-analysis of transcriptome datasets. Sci Rep 2017; 7:9719-[PMID: 28852117].

23. Riddell N, Crewther SG. Integrated comparison of gwas, transcriptome, and proteomics studies highlights similarities in the biological basis of animal and human myopia. Invest Ophthalmol Vis Sci 2017; 58:660-9. [PMID: 28135361].

24. Shih Y-F, Fitzgerald ME, Norton TT, Gamlin PD, Hodos W, Reiner A. Reduction in choroidal blood flow occurs in chicks wearing goggles that induce eye growth toward myopia. Curr Eye Res 1993; 12:219-27. [PMID: 8482110].

25. Jin N, Stjernschantz J. Regional blood flow in the myopic chick eye during and after form deprivation: A study with radioactively-labelled microspheres. Exp Eye Res 2000; 71:233-8. [PMID: 10973732].

26. Wildsoet C, Wallman J. Choroidal and scleral mechanisms of compensation for spectacle lenses in chicks. Vision Res 1995; 35:1175-94. [PMID: 7610579].

27. Rappsilber J, Ishihama Y, Mann M. Stop and go extraction tips for matrix-assisted laser desorption/ionization, nanoelectrospray, and lc/ms sample pretreatment in proteomics. Anal Chem 2003; 75:663-70. [PMID: 12585499].

28. Cox J, Mann M. Maxquant enables high peptide identification rates, individualized p.P.B.-range mass accuracies and proteome-wide protein quantification. Nat Biotechnol 2008; 26:1367-72. [PMID: 19029910].

29. Cox J, Hein MY, Luber CA, Paron I, Nagaraj N, Mann M. Accurate proteome-wide label-free quantification by delayed normalization and maximal peptide ratio extraction, termed maxlfq. Mol Cell Proteomics 2014; 13:2513-26. [PMID: 24942700].

30. Ritchie ME, Phipson B, Wu D, Hu Y, Law CW, Shi W, Smyth GK. Limma powers differential expression analyses for rna-sequencing and microarray studies. Nucleic Acids Res 2015; 43:e47-[PMID: 25605792].

31. Mi H, Muruganujan A, Casagrande JT, Thomas PD. Large-scale gene function analysis with the panther classification system. Nat Protoc 2013; 8:1551-66. [PMID: 23868073].

32. Benjamini Y, Hochberg Y. Controlling the false discovery rate: A practical and powerful approach to multiple testing. J J R Stat Soc Series B Stat Methodol 1995:289–300.

33. Sonnhammer EL, Ostlund G. Inparanoid 8: Orthology analysis between 273 proteomes, mostly eukaryotic. Nucleic Acids Res 2015; 43:D234-9. [PMID: 25429972].

34. Altenhoff AM, Boeckmann B, Capella-Gutierrez S, Dalquen DA, Deluca T, Forslund K, Huerta-Cepas J, Linard B, Pereira C, Pryszcz LP, Schreiber F, Da Silva AS, Szklarczyk D, Train CM, Bork P, Lecompte O, Von Mering C, Xenarios I, Sjolander K, Jensen LJ, Martin MJ, Muffato M. Quest for Orthologs C, Gabaldon T, Lewis SE, Thomas PD, Sonnhammer E, Dessimoz C. Standardized benchmarking in the quest for orthologs. Nat Methods 2016; 13:425-30. [PMID: 27043882].

35. Smedley D, Haider S, Ballester B, Holland R, London D, Thorisson G, Kasprzyk A. Biomart–biological queries made easy. BMC Genomics 2009; 10:22-[PMID: 19144180].

36. Torii H, Kurihara T, Seko Y, Negishi K, Ohnuma K, Inaba T, Kawashima M, Jiang X, Kondo S, Miyauchi M. Violet light exposure can be a preventive strategy against myopia progression. EBioMedicine 2017; 15:210-9. [PMID: 28063778].

37. Riddell N, Giummarra L, Hall N, Crewther S. Bidirectional expression of metabolic, structural, and immune pathways in early myopia and hyperopia. Front Neurosci 2016; 10:[PMID: 27625591].

38. Metlapally R, Park HN, Chakraborty R, Wang KK, Tan CC, Light JG, Pardue MT, Wildsoet CF. Genome-wide scleral micro-and messenger-rna regulation during myopia

development in the mouse. Invest Ophthalmol Vis Sci 2016; 57:6089-97. [PMID: 27832275].

39. Walter W, Sanchez-Cabo F, Ricote M. Goplot: An r package for visually combining expression data with functional analysis. Bioinformatics 2015; 31:2912-4. [PMID: 25964631].

40. Szklarczyk D, Morris JH, Cook H, Kuhn M, Wyder S, Simonovic M, Santos A, Doncheva NT, Roth A, Bork P, Jensen LJ, Von Mering C. The string database in 2017: Quality-controlled protein-protein association networks, made broadly accessible. Nucleic Acids Res 2017; 45:D1D362-8. [PMID: 27924014].

41. Köhler S, Vasilevsky NA, Engelstad M, Foster E, Mcmurry J, Ayme S, Baynam G, Bello SM, Boerkoel CF, Boycott KM, Brudno M, Buske OJ, Chinnery PF, Cipriani V, Connell LE, Dawkins HJ, Demare LE, Devereau AD, De Vries BB, Firth HV, Freson K, Greene D, Hamosh A, Helbig I, Hum C, Jahn JA, James R, Krause R, Sj FL, Lochmuller H, Lyon GJ, Ogishima S, Olry A, Ouwehand WH, Pontikos N, Rath A, Schaefer F, Scott RH, Segal M, Sergouniotis PI, Sever R, Smith CL, Straub V, Thompson R, Turner C, Turro E, Veltman MW, Vulliamy T, Yu J, Von Ziegenweidt J, Zankl A, Zuchner S, Zemojtel T, Jacobsen JO, Groza T, Smedley D, Mungall CJ, Haendel M, Robinson PN. The human phenotype ontology in 2017. Nucleic Acids Res 2017; 45:D1D865-76. [PMID: 27899602].

42. Robinson PN, Kohler S, Bauer S, Seelow D, Horn D, Mundlos S. The human phenotype ontology: A tool for annotating and analyzing human hereditary disease. Am J Hum Genet 2008; 83:610-5. [PMID: 18950739].

43. Merico D, Isserlin R, Stueker O, Emili A, Bader GD. Enrichment map: A network-based method for gene-set enrichment visualization and interpretation. PLoS One 2010; 5:e13984-[PMID: 21085593].

44. Subramanian A, Kuehn H, Gould J, Tamayo P, Mesirov JP. Gsea-p: A desktop application for gene set enrichment analysis. Bioinformatics 2007; 23:3251-3. [PMID: 17644558].

45. McGlinn AM, Baldwin DA, Tobias JW, Budak MT, Khurana TS, Stone RA. Form-deprivation myopia in chick induces limited changes in retinal gene expression. Invest Ophthalmol Vis Sci 2007; 48:3430-6. [PMID: 17652709].

46. Stone RA, Mcglinn AM, Baldwin DA, Tobias JW, Iuvone PM, Khurana TS. Image defocus and altered retinal gene expression in chick: Clues to the pathogenesis of ametropia. Invest Ophthalmol Vis Sci 2011; 52:5765-77. [PMID: 21642623].

47. Ashby RS, Feldkaemper MP. Gene expression within the amacrine cell layer of chicks after myopic and hyperopic defocus. Invest Ophthalmol Vis Sci 2010; 51:3726-35. [PMID: 20207967].

48. Schippert R, Schaeffel F, Feldkaemper MP. Microarray analysis of retinal gene expression in chicks during imposed myopic defocus. Mol Vis 2008; 14:1589-[PMID: 18769560].

49. Wu Y, Liu Q, To CH, Li KK, Chun RKM, Yu JFJ, Lam TC. Differential retinal protein expressions during form deprivation myopia in albino guinea pigs. Curr Proteomics 2014; 11:37-47. .

50. Zhou X, Ye J, Willcox MD, Xie R, Jiang L, Lu R, Shi J, Bai Y, Qu J. Changes in protein profiles of guinea pig sclera during development of form deprivation myopia and recovery. Mol Vis 2010; 16:2163-74. [PMID: 21139681].

51. Frost MR, Norton TT. Alterations in protein expression in tree shrew sclera during development of lens-induced myopia and recovery. Invest Ophthalmol Vis Sci 2012; 53:322-36. [PMID: 22039233].

52. Frost MR, Norton TT. Differential protein expression in tree shrew sclera during development of lens-induced myopia and recovery. Mol Vis 2007; 13:1580-8. [PMID: 17893659].

53. Barathi VA, Chaurasia SS, Poidinger M, Koh SK, Tian D, Ho C, Iuvone PM, Beuerman RW, Zhou L. Involvement of gaba transporters in atropine-treated myopic retina as revealed by itraq quantitative proteomics. J Proteome Res 2014; 13:4647-58. [PMID: 25211393].

54. Li S, Wu JS, Ding H, Liao AP, He H, Stell WK, Zhong XW. Flicker downregulates the content of crystallin proteins in form-deprived c57bl/6 mouse retina. Exp Eye Res 2012; 101:1-8. [PMID: 22659691].

55. Brand C, Schaeffel F, Feldkaemper MP. A microarray analysis of retinal transcripts that are controlled by image contrast in mice. Mol Vis 2007; 13:920-32. [PMID: 17653032].

56. Tkatchenko AV, Walsh PA, Tkatchenko TV, Gustincich S, Raviola E. Form deprivation modulates retinal neurogenesis in primate experimental myopia. Proc Natl Acad Sci USA 2006; 103:4681-6. [PMID: 16537371].

57. Jovanovic M, Rooney MS, Mertins P, Przybylski D, Chevrier N, Satija R, Rodriguez EH, Fields AP, Schwartz S, Raychowdhury R, Mumbach MR, Eisenhaure T, Rabani M, Gennert D, Lu D, Delorey T, Weissman JS, Carr SA, Hacohen N, Regev A. Immunogenetics. Dynamic profiling of the protein life cycle in response to pathogens. Science 2015; 347:1259038-[PMID: 25745177].

58. Li JJ, Biggin MD. Gene expression. Statistics requantitates the central dogma. Science 2015; 347:1066-7. [PMID: 25745146].

59. Li JJ, Bickel PJ, Biggin MD. System wide analyses have underestimated protein abundances and the importance of transcription in mammals. PeerJ 2014; 2:e270-[PMID: 24688849].

60. Teakle EM, Wildsoet CF, Vaney DI. The spatial organization of tyrosine hydroxylase-immunoreactive amacrine cells in the chicken retina and the consequences of myopia. Vision Res 1993; 33:2383-96. [PMID: 7902629].

61. Troilo D, Xiong M, Crowley JC, Finlay BL. Factors controlling the dendritic arborization of retinal ganglion cells. Vis Neurosci 1996; 13:721-33. [PMID: 8870228].

62. Beresford JA, Crewther SG, Kiely PM, Crewther DP. Comparison of refractive state and circumferential morphology of retina, choroid, and sclera in chick models of experimentally induced ametropia. Optom Vis Sci 2001; 78:40-9. [PMID: 11233334].

63. Lam TC, Li KK, Lo SCL, Guggenheim JA, To CH. Application of fluorescence difference gel electrophoresis technology in searching for protein biomarkers in chick myopia. J Proteome Res 2007; 6:4135-49. [PMID: 17924678].

64. Tkatchenko AV, Luo X, Tkatchenko TV, Vaz C, Tanavde VM, Maurer-Stroh S, Zauscher S, Gonzalez P, Young TL. Large-scale microrna expression profiling identifies putative retinal mirna-mrna signaling pathways underlying form-deprivation myopia in mice. PLoS One 2016; 11:e0162541-[PMID: 27622715].

65. Steingrimsson E, Copeland NG, Jenkins NA. Melanocytes and the microphthalmia transcription factor network. Annu Rev Genet 2004; 38:365-411. [PMID: 15568981].

66. Graw J. The genetic and molecular basis of congenital eye defects. Nat Rev Genet 2003; 4:876-88. [PMID: 14634635].

67. D'mello SA, Finlay GJ, Baguley BC, Askarian-Amiri ME. Signaling pathways in melanogenesis. Int J Mol Sci 2016; 17:[PMID: 27428965].

68. Nathan J, Kiely P, Crewther S, Crewther D. Disease-associated visual image degradation and spherical refractive errors in children. Am J Optom Physiol Opt 1985; 62:680-8. [PMID: 4073201].

69. Wildsoet CF, Oswald PJ, Clark S. Albinism: Its implications for refractive development. Invest Ophthalmol Vis Sci 2000; 41:1-7. [PMID: 10634592].

70. Wang JY, Liu SZ, Wei X, Wu XY, Tan XP. High myopia and retinal ultrastructure of albino guinea-pigs. Journal of Central South University Medical Sciences 2007; 32:282-7. [PMID: 17478937].

71. Rymer J, Choh V, Bharadwaj S, Padmanabhan V, Modilevsky L, Jovanovich E, Yeh B, Zhang Z, Guan H, Payne W, Wildsoet CF. The albino chick as a model for studying ocular developmental anomalies, including refractive errors, associated with albinism. Exp Eye Res 2007; 85:431-42. [PMID: 17651735].

72. Hu D-N, Roberts JE, Mccormick SA. Role of uveal melanocytes in the development of myopia. In Lin LK., Yung-Feng Shih., Hung PT, editors. Myopia updates II: Tokyo: Springer; 2000. p. 125–6.

73. Kishi H, Kuroda E, Mishima HK, Yamashita U. Role of TGF-beta in the retinoic acid-induced inhibition of proliferation and melanin synthesis in chick retinal pigment epithelial cells in vitro. Cell Biol Int 2001; 25:1125-9. [PMID: 11913956].

74. Kajimoto H, Hashimoto K, Bonnet SN, Haromy A, Harry G, Moudgil R, Nakanishi T, Rebeyka I, Thébaud B, Michelakis ED. Oxygen activates the rho/rho-kinase pathway and induces rhob and rock-1 expression in human and rabbit ductus arteriosus by increasing mitochondria-derived reactive oxygen species. Circulation 2007; 115:1777-88. [PMID: 17353442].

75. Pinti M, Gibellini L, Liu Y, Xu S, Lu B, Cossarizza A. Mitochondrial lon protease at the crossroads of oxidative stress, ageing and cancer. Cell Mol Life Sci 2015; 72:4807-24. [PMID: 26363553].

76. Chen PJ, Huang YS. Cpeb2-eef2 interaction impedes hif-1alpha rna translation. EMBO J 2012; 31:959-71. [PMID: 22157746].

77. Soliman D, Hamming KS, Matemisz LC, Light PE. Reactive oxygen species directly modify sodium-calcium exchanger activity in a splice variant-dependent manner. J Mol Cell Cardiol 2009; 47:595-602. [PMID: 19481548].

78. Chondrogianni N, Stratford FL, Trougakos IP, Friguet B, Rivett AJ, Gonos ES. Central role of the proteasome in senescence and survival of human fibroblasts: Induction of a senescence-like phenotype upon its inhibition and resistance to stress upon its activation. J Biol Chem 2003; 278:28026-37. [PMID: 12736271].

79. Kwak MK, Wakabayashi N, Greenlaw JL, Yamamoto M, Kensler TW. Antioxidants enhance mammalian proteasome expression through the keap1-nrf2 signaling pathway. Mol Cell Biol 2003; 23:8786-94. [PMID: 14612418].

80. Yaung J, Jin M, Barron E, Spee C, Wawrousek EF, Kannan R, Hinton DR. Alpha-crystallin distribution in retinal pigment epithelium and effect of gene knockouts on sensitivity to oxidative stress. Mol Vis 2007; 13:566-77. [PMID: 17438522].

81. Wong WM, Gerry AB, Putt W, Roberts JL, Weinberg RB, Humphries SE, Leake DS, Talmud PJ. Common variants of apolipoprotein a-iv differ in their ability to inhibit low density lipoprotein oxidation. Atherosclerosis 2007; 192:266-74. [PMID: 16945374].

82. Sandbach JM, Coscun PE, Grossniklaus HE, Kokoszka JE, Newman NJ, Wallace DC. Ocular pathology in mitochondrial superoxide dismutase (sod2)-deficient mice. Invest Ophthalmol Vis Sci 2001; 42:2173-8. [PMID: 11527927].

83. Fukui M, Zhu BT. Mitochondrial superoxide dismutase sod2, but not cytosolic sod1, plays a critical role in protection against glutamate-induced oxidative stress and cell death in ht22 neuronal cells. Free Radic Biol Med 2010; 48:821-30. [PMID: 20060889].

84. Tezel G, Yang X, Luo C, Cai J, Kain AD, Powell DW, Kuehn MH, Pierce WM. Hemoglobin expression and regulation in glaucoma: Insights into retinal ganglion cell oxygenation. Invest Ophthalmol Vis Sci 2010; 51:907-19. [PMID: 19741249].

85. Tezel TH, Geng L, Lato EB, Schaal S, Liu Y, Dean D, Klein JB, Kaplan HJ. Synthesis and secretion of hemoglobin by retinal pigment epithelium. Invest Ophthalmol Vis Sci 2009; 50:1911-9. [PMID: 19060278].

86. Wulf MA, Senatore A, Aguzzi A. The biological function of the cellular prion protein: An update. BMC Biol 2017; 15:34-[PMID: 28464931].

87. Ho EC, Lam KS, Chen YS, Yip JC, Arvindakshan M, Yamagishi S, Yagihashi S, Oates PJ, Ellery CA, Chung SS, Chung SK. Aldose reductase-deficient mice are protected from delayed motor nerve conduction velocity, increased c-jun nh2-terminal kinase activation, depletion of reduced glutathione, increased superoxide accumulation, and DNA damage. Diabetes 2006; 55:1946-53. [PMID: 16804062].

88. Stamer K, Vogel R, Thies E, Mandelkow E, Mandelkow EM. Tau blocks traffic of organelles, neurofilaments, and app vesicles in neurons and enhances oxidative stress. J Cell Biol 2002; 156:1051-63. [PMID: 11901170].

89. Feng Z, Liu Z, Li X, Jia H, Sun L, Tian C, Jia L, Liu J. Alpha-tocopherol is an effective phase ii enzyme inducer: Protective effects on acrolein-induced oxidative stress and mitochondrial dysfunction in human retinal pigment epithelial cells. J Nutr Biochem 2010; 21:1222-31. [PMID: 20153624].

90. Yadavilli S, Mayo LD, Higgins M, Lain S, Hegde V, Deutsch WA. Ribosomal protein s3: A multi-functional protein that interacts with both p53 and mdm2 through its kh domain. DNA Repair (Amst) 2009; 8:1215-24. [PMID: 19656744].

91. Meyer RC, Giddens MM, Schaefer SA, Hall RA. Gpr37 and gpr37l1 are receptors for the neuroprotective and glioprotective factors prosaptide and prosaposin. Proc Natl Acad Sci USA 2013; 110:9529-34. [PMID: 23690594].

92. Yildirim Z, Ucgun NI, Yildirim F. The role of oxidative stress and antioxidants in the pathogenesis of age-related macular degeneration. Clinics (Sao Paulo) 2011; 66:743-6. [PMID: 21789374].

93. Biesemeier A, Yoeruek E, Eibl O, Schraermeyer U. Iron accumulation in bruch's membrane and melanosomes of donor eyes with age-related macular degeneration. Exp Eye Res 2015; 137:39-49. [PMID: 26026877].

94. Blasiak J, Petrovski G, Veréb Z, Facskó A, Kaarniranta K. Oxidative stress, hypoxia, and autophagy in the neovascular processes of age-related macular degeneration. BioMed Res Int 2014; 2014:768026-[PMID: 24707498].

95. Hendriks M, Verhoeven VJ, Buitendijk GH, Polling JR, Meester-Smoor MA, Hofman A, Van Huet R, Oomen C, Plomp A, Van Genderen M. Development of refractive errors–what can we learn from inherited retinal dystrophies? Am J Ophthalmol 2017; 182:81-9. [PMID: 28751151].

96. Flitcroft DI, Loughman J, Wildsoet CF, Williams C, Guggenheim JA. Novel Myopia Genes and Pathways identified from Syndromic Forms of Myopia. Invest Ophthalmol Vis Sci 2017; 58:5480-.

97. Wisely CE, Sayed JA, Tamez H, Zelinka C, Abdel-Rahman MH, Fischer AJ, Cebulla CM. The chick eye in vision research: An excellent model for the study of ocular disease. Prog Retin Eye Res 2017; 61:72-97. [PMID: 28668352].

Articles are provided courtesy of Emory University and the Zhongshan Ophthalmic Center, Sun Yat-sen University, P.R. China. The print version of this article was created on 5 December 2017. This reflects all typographical corrections and errata to the article through that date. Details of any changes may be found in the online version of the article.